Original Article

Metal Artifact Suppression in Dental Cone Beam Computed Tomography Images Using Image Processing Techniques

Abstract

Background: Dental cone beam computed tomography (CBCT) images suffer from severe metal artifacts. These artifacts degrade the quality of acquired image and in some cases make it unsuitable to use. Streaking artifacts and cavities around teeth are the main reason of degradation. **Methods:** In this article, we have proposed a new artifact reduction algorithm which has three parallel components. The first component extracts teeth based on the modeling of image histogram with a Gaussian mixture model. Striking artifact reduction component reduces artifacts using converting image into the polar domain and applying morphological filtering. The third component fills cavities through a simple but effective morphological filtering operation. **Results:** Finally, results of these three components are combined into a fusion step to create a visually good image which is more compatible to human visual system. **Conclusions:** Results show that the proposed algorithm reduces artifacts of dental CBCT images and produces clean images.

Keywords: *Artifact reduction, cone beam computed tomography, dental images, morphological filtering*

Masoumeh Johari, Milad Abdollahzadeh[1], Farzad Esmaeili, Vahideh Sakhamanesh

Department of Oral and Maxillofacial Radiology, Dental and Periodontal Research Center, Faculty of Dentistry, Tabriz University of Medical Sciences, [1]Department of Communications Engineering, Faculty of Electrical and Computer Engineering, University of Tabriz, Tabriz, Iran

Introduction

Nowadays, three-dimensional (3D) imaging is one of the successful clinical applications. This imaging method has many advantages compared to the two-dimensional X-ray imaging and it is used as an important tool to evaluate the condition of the internal structures and organs. Among the other imaging methods, cone beam computed tomography (CBCT) imaging technique is a secure and reliable diagnostic method.[1] At the inception of the second decade of this century, CBCT machines are extensively presented in many states of the world. CBCT images are ruined with artifacts affected by high-density matters such as metal implants, dental fillings, or surgical clips. Such high-density objects generate distinguished streak-like artifacts and shadows in CBCT images and hamper clinical applications, for example, radiation therapy treatment planning.[2] Supporting high-resolution 3D imaging of stiff tissues at a low radiation dose, CBCT has verified to be beneficial in many dental parts such as endodontics and orthodontics.[1] IN addition, several authors have studied metal artifact lessening using modified scanning methods.[3]

In spite of improvements in imaging methods, researchers are faced with various problems. One of the problems is that high-density objects exist in CBCT images such as metal implants and dental fillings and create a lot of artifacts. Metal artifacts are one of the numerous forms of artifacts observed in all kinds of CT imaging.[4] Metal artifacts stay a challenge for CT remodeling. The streaking artifacts affected by metal will critically reduce the image quality, which may seriously increase the difficulty of diagnosis.[5] A raising number of CBCT devices have become existing over the last few years, displaying an extensive range in exposure parameters such as field of view size, beam quality, amount of X-rays, and rotation arc. Furthermore, different sizes and types of detectors are used, and different reconstruction algorithms are applied. All these constraints influence the diagnostic image aspect in terms of image noise, high- and low-contrast resolution, and artifacts.[6,7]

Most of these researches use viewers to estimate artifact-associated parameters, which can be valuable to measure artifact lessening and diagnostic effects. However, this type of subjective estimation cannot

How to cite this article: Johari M, Abdollahzadeh M, Esmaeili F, Sakhamanesh V. Metal artifact suppression in dental cone beam computed tomography images using image processing techniques. J Med Sign Sens 2018;8:12-24.

Address for correspondence:
Dr. Vahideh Sakhamanesh, Department of Oral and Maxillofacial Radiology, Dental and Periodontal Research Center, Faculty of Dentistry, Tabriz University of Medical Sciences, Tabriz, Iran. E-mail: dr.v.sakhamanesh@gmail.com

Website: www.jmss.mui.ac.ir

prepare a comparison of the effect of altered devices and procedures and cannot be used in routine quality control. Some researchers have evaluated the quantification of metal artifacts using different attitudes.[8,9]

CBCT metal artifact lessening has a problem that the metallic substances in a human body have higher attenuation ratios than that of soft tissues and generate displeasing artifacts such as streak, noise, and shaded artifacts. These artifacts considerably reduce the graphical quality of the image and alter the skeletal structure close to metallic substances. The two key causes to generate metal artifacts are photon starvation and beam solidification. The number of photons, which move through the metallic matters, is not as much of as the number of photons crossing through the nonmetallic matters. The noise and scatter generate streak artifacts in a reassembled CT image.[10]

The purpose of this study is to suppress metal artifacts in dental CBCT images to reconstruct suitable images with fewer artifacts and better visual quality. We have proposed an algorithm which is completely independent of scanning (data acquisition) and uses image processing techniques to reduce artifacts. This algorithm reduces streaking artifacts and fills cavities of dental CBCT images without distorting of valuable information in dental area. Considering independency of this algorithm from data acquisition part, it can be used along with other artifact reduction algorithms which modify scanning algorithm to reduce artifacts.

The remaining parts of the article are as follows: proposed algorithm section presents the proposed dental CBCT artifact reduction algorithm. The results section provides results of applying proposed algorithm and its evaluation. The article is concluded in conclusion section.

Proposed Algorithm

As mentioned before, dental CBCT images suffer from streaking artifacts and cavities around teeth. The proposed algorithm tries to overcome these problems. The overall structure of the proposed algorithm is shown in Figure 1.

As demonstrated in Figure 1, there are three parallel parts in the first step. In teeth extraction part, teeth are recognized and extracted through a histogram-based thresholding and morphological filtering. In order to automate this procedure, histogram of the image is modeled as a Gaussian mixture model (GMM) and threshold is defined based on the parameters of the GMM. In streaking artifact reduction part, images are transferred into polar domain in order to convert streaking artifacts into vertical lines. Then, an adaptive morphological filtering is applied to eliminate these artifacts. Gray-level values of pixels in cavity regions correspond to the set of regional minima in the dental CBCT image which is similar to the definition of holes in the morphological image processing.[11] Usually, cavity regions of dental CBCT images do not include complex

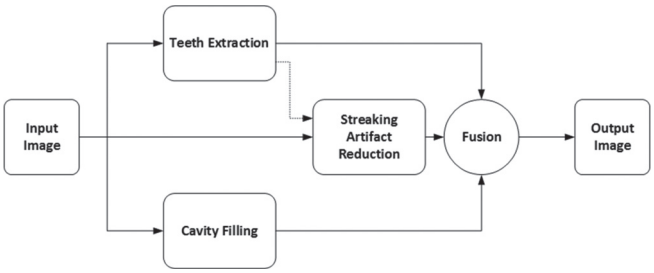

Figure 1: Proposed algorithm for increasing subjective quality of dental cone beam computed tomography images

texture or image features. Therefore, we have used simple morphological filling algorithm to fill these areas based on the neighborhood information. After these three parts, a fusion step is applied to create a single image which includes benefits of all steps. The output of fusion step is a clean and artifact-free image. In the next subsections, each step has been explained in more detail. In order to show the effectiveness of each proposed step, a visual result of applying it on a single image is included.

Teeth extraction

In this part, we have proposed a method based on the image histogram to calculate a threshold value for teeth extraction. Gray scale value (intensity value) and the shape of teeth are used to segment these areas. The main procedure is to produce a binary image using thresholding and then refine that binary image by morphological filtering. In the thresholding, each pixel value is replaced with a black pixel if the image intensity is less than some predefined threshold, or a white pixel if the image intensity is greater than that threshold. The predefined value of threshold has great effect on the final result. In dental CBCT images, the intensity value of streaking artifacts is near to the intensity value of the teeth area. Therefore, we need to choose the threshold accurately. In this section, we have proposed a method which uses histogram of dental CBCT images to define an accurate threshold value. This threshold value decreases the amount of remaining streaking artifacts after thresholding. Suppose that $I = (I[i, j];\ 1 \le i \le M;\ 1 \le j \le N)$ is a digital image where $I(i, j)$ denotes the gray-level value (intensity value) of the image at a pixel in i^{th} row and j^{th} column and M and N denote the number of rows and columns, respectively, then the total number of pixels in the image is $M \times N$. Suppose that image intensity is digitized into L levels that are $(I_0, I_1, \ldots, I_{L-1})$ therefore, it is obvious that . If the total number of pixels with gray level of I_k equals to n_k, the probability density function (PDF) of I_k is as follows:

$$p(I_k) = \frac{n_k}{M \times N};\ k = 0,1,\ldots,L \quad (1)$$

The graphical demonstration of $p(I_k)$ versus I_k is defined as an image histogram.[12] Therefore, the image histogram shows frequency of appearance of each gray level on that image. The most popular number of levels in

a digital image is $L = 256$ which means it requires 8 bits to represent the value of each pixel. In dental CBCT images, gray-level values of most of the pixels are concentrated on three parts. Figure 2 shows a dental CBCT image together with its histogram.

Algorithm 1: Histogram extension

01: $center = 0, \Delta = 20$

02: $while\ \Delta > 10\ do$

03: $n = 1$

04: $x(center + n) = x(center - n)$

05: $\Delta = \left| x(center + n) - x(center + n - 1) \right|$

06: $n = n + 1$

07: *end while*

08: $center = 255, \Delta = 20$

09: $while\ \Delta > 10\ do$

10: $n = 1$

11: $x(center - n) = x(center + n)$

12: $\Delta = \left| x(center - n) - x(center - n + 1) \right|$

13: $n = n + 1$

14: *end while*

Considering Figure 2b, the main intensity values are clustered in three regions. Background and cavities are shown in black, which corresponds to the near-zero peak in histogram. Mouth tissue is shown in gray, which corresponds to the second peak around 70. Finally, enamel, dentin, and metal objects are shown in white, which corresponds to the third peak around 255. Streaking artifacts have intensity values between the second and third peaks. In some cases, the intensity value of streaking artifacts is near to the value of dental parts. Therefore, we need to use an accurate threshold value to segment teeth area. Proper modeling of histogram can help us to obtain the desired threshold value.

Based on the shape of histogram, we have proposed to model that using GMM.[13] However, since only half of the Gaussian shape peaks exists in the first and third peaks, we have extended histogram of image to get a modified one.

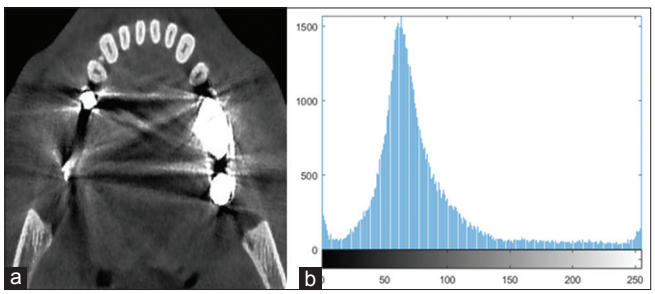

Figure 2: Cone beam computed tomography dental image and its histogram (a) dental cone beam computed tomography image, (b) related histogram

This modified histogram makes it easier to model it using GMM. To do this, we have extended histogram using algorithm 1. Algorithm 1 extends the first and third peaks of the histogram by duplicating data symmetrically with regard to $n = 0$ and $n = 255$, respectively. Extension continues until the difference between successive data samples gets smaller than a predefined threshold . The result of extending histogram of Figure 2 is shown in Figure 3.

Using extended histogram, we can model it as GMM. A one-dimensional GMM[14] is a weighted sum of M component Gaussian densities as given by Eq. 2 as follows:

$$p(x|\lambda) = \sum_{i=1}^{M} \omega_i g(x \mid \mu_i, \sigma_i) \tag{2}$$

where x is data vector, $\omega_i; i = 1.....M$ are the mixture weights and $g(x|\mu_i.\sigma_i); i = 1.....M$ are the component Gaussian densities. Each component density is a one-dimensional Gaussian function of the form:

$$g(x|\mu_i, \sigma_i) = \frac{1}{\sqrt{2\pi}\sigma_i} \exp\left\{ -\frac{(x - \mu_i)^2}{2\sigma_i^2} \right\} \tag{3}$$

with a mean of μ_i and standard deviation (SD) of σ_i. The complete GMM is defined by the mean, SD, and mixture weight of each component:

$$\lambda = \{\mu_i, \sigma_i, \omega_i\}\ ; i = 1, \ldots, M \tag{4}$$

where λ is the set of the GMM parameters. Modified histogram of CBCT images contains three peaks which yield $M = 3$. We have used expectation maximization[15] algorithm to obtain . After finding GMM model parameters, we use them to obtain threshold value. The main challenge in the determining threshold value is that the intensity value of some streaking artifacts is so close to the intensity value of teeth region. Therefore, inaccurate value of threshold transfers these artifacts into the binary image and degrades the final result of teeth extraction procedure. We need to find threshold value in a way to surpass streaking artifacts and retain teeth regions. Based on our data set, we found it empirically that after finding GMM parameters, the best place to set our threshold is given as follows:

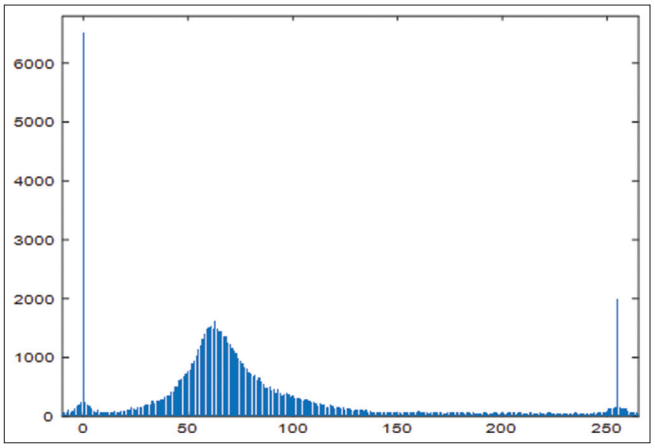

Figure 3: Extended histogram

$$\text{Threshold} = \frac{(\mu_2 + 2\sigma_2) + (\mu_3 - 2\sigma_3)}{2} \quad (5)$$

This threshold is used to convert gray-scale image into the binary image. In order to obtain binary image, pixels with value higher than (5) will be mapped to 1 and the remaining will be mapped to 0. After obtaining binary image, morphological opening is used to remove irrelevant objects and obtain a mask which contains teeth. Morphological opening (described with more details in morphological filtering section) includes an erosion followed by dilation. Erosion operation removes objects that are smaller than structuring element and dilation operation restores the shape of the remaining objects. We use a disk-shaped structuring element in morphological opening due to the disk-like shape of teeth. After obtaining the mask, we use a simple element-by-element multiplication to obtain the final result of the teeth extraction.

Figure 4a shows the result of teeth extraction using proposed method. As one can see, original image in Figure 2a includes severe streaking artifacts with intensity values close to the intensity values of teeth. However, the proposed threshold selection method surpasses considerable part of streaking artifacts and extracts teeth accurately. Result of teeth extraction using the threshold provided by the popular method of Otsu[16] is shown in Figure 4b. This method derives threshold by maximizing the discriminant measure of the resultant classes in gray levels of image. As one can see, the conventional method for obtaining threshold transfers some undesirable streaking artifacts into the final images.

Streaking artifact reduction

Thickness and orientation of streaking artifacts in a CBCT images are quite different. Therefore, inaccurate use of filtering may cause severe distortions in output image. Streaking artifacts show some degree of symmetry since the image is derived from the scattering values of X-ray beam rotating around the object. Such a problem is also investigated in the study by Naranjo *et al*.[17] for CT images where authors transferred CT image into the polar domain to facilitate artifact reduction procedure. Images are transformed into the polar domain using symmetry origin as transform center. In this way, all the related streaking artifacts are transferred into almost vertical lines in polar domain. We have used similar algorithm with some improvements. Block diagram of the proposed method for streaking artifact reduction is shown in Figure 5.

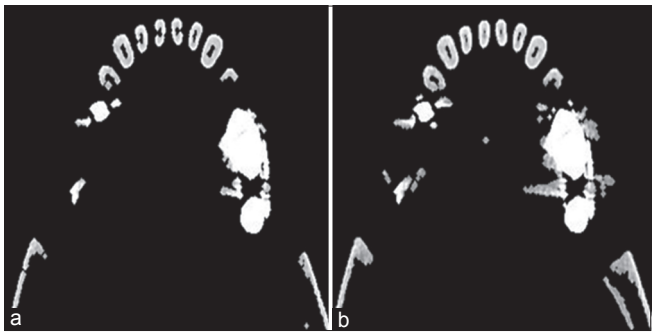

Figure 4: Extracted teeth using (a) proposed method, (b) conventional method of Otsu

First, streaking origins of the input image are detected. Input image is transferred into the polar domain considering each one of the streaking origins as a transfer center. Then, adaptive morphological opening operation is applied in horizontal direction to eliminate streaking artifacts. Finally, artifact-reduced image is transferred into the Cartesian domain using polar to Cartesian transform.

Automated streaking artifact origin detection

In the study by Naranjo *et al.*,[17] the origin of streaking artifacts is detected using granulometry-based line detection and curve fitting. In textured image processing, granulometry refers to the extraction of sets of elements with some specific properties in an image.[18] The image is processed by a filtering scheme so that in each step some structures are extracted and refined. In the study by Naranjo *et al.*,[17] the filtering is done by morphological operators. The structural element shape, size, and orientation in these morphological operators are specialized into the CT images which were used in the study by Naranjo *et al*.[17] Therefore, the algorithm cannot be generalized into the other types of data bases including dental CBCT images. On the other hand, this method can detect only one streaking artifact center. In a case where there are several metallic objects, human intervention is required where a bounding box must be defined around each streaking artifact source. Therefore, this method is not fully automatic and needs some supervision to work correctly.

To solve these problems, we have proposed a new method which can detect multiple streaking artifact sources in a single image. Rather than using morphological-based granulometry, we have used image features together with Radon transform to detect lines. In this way, line detection is done based on image features which can be applied to various types of images. In the study by Naranjo *et al.*,[17] it has been proposed that morphological filtering enhances the lines on the region of interest (one of the streaking sources which was determined by bonding box) and destroys others. However, image feature-based line detection can detect the lines in the whole image. Then, we use curve fitting to find line intersections as streaking origins.

Proposed algorithm for streaking artifact origin detection is shown in Figure 6. The first edges of input image are extracted. We use Sobel edge detection[19] due to good balance between complexity and accuracy. Then, the Radon transform of resulted edge map is calculated. The Radon transform of a function $g(x, y)$ in two-dimensional (2D) space is defined as follows:[20]

Figure 5: Block diagram of proposed method for streaking artifact reduction

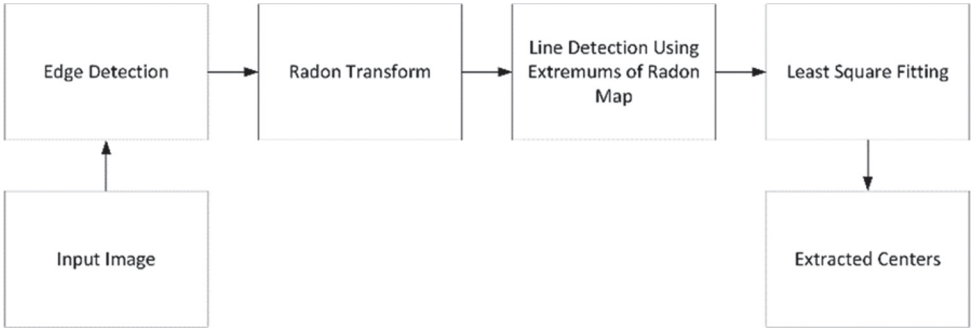

Figure 6: Block diagram of proposed method for streaking artifact centers

$$R(\rho,\theta)=\int_{-\infty}^{\infty}\int_{-\infty}^{\infty} g(x,y)\,\delta(\rho-x\cos\theta-y\sin\theta)\,dxdy \tag{6}$$

where $\delta(x)$ is the Dirac function which is infinite for zero argument and zero for the other arguments and it integrates to one. The term $\delta(\rho-x\cos\theta-y\sin\theta)$ forces the integration of $g(x, y)$ along the line defined by:

$$\rho-x\cos\theta-y\sin\theta=0 \tag{7}$$

Consequently, if $g(x, y)$ is a 2D image intensity function, computation of its Radon transform yields the projection across the image at varying orientations θ and offsets ρ, which is relative to a parallel line passing through the image center.[21] Therefore, the Radon transform of image edge map contains a peak corresponding to every line in the image that is brighter than its surrounding and a valley for every dark line. Using these extremum points, we can detect location and orientation of each line in original image.[22] Figure 7b shows the Radon transform for the edge map of the input image shown in Figure 7a. In Figure 7b, vertical axis shows distance (ρ in Eq. 6) and horizontal axis shows orientation (θ in Eq. 6). Streaking artifacts marked in Figure 7a correspond to the maxima points marked in Figure 7b. After detecting each line, intersections of lines are calculated using slope-intercept form of equation for each possible couple of lines. Finally, a point is a streaking artifact origin when there are at least N_{int} intersection points in its neighborhood and it is located on the teeth region which is described in teeth extraction section. We have used N_{int} = 3 in our simulations which is the best choice based on our data set.

Figure 8 shows the result of applying this algorithm into the dental CBCT image shown in Figure 2a. Figure 8a shows detected lines using extremum points of Radon transform. As one can see, there are five intersections of lines in this image. However, one of them is not placed on the teeth location [Figure 4a] which will not be included. Finally, the detected streaking artifact origins are shown in Figure 8b. Based on the results shown in Figure 8b, our method can detect streaking artifact origins in an automated way.

Polar coordinate

As mentioned before, streaking artifacts scattered in a symmetric way around metal matter (streaking artifact origin). Based on the properties of polar domain, transferring CBCT image using streaking artifact origin as a transform center maps these lines into the vertical lines in a new domain. This makes it easy to remove artifacts with filtering operation. Therefore, after calculating streaking artifacts' origin, input image is transferred into the polar domain using each origin as a transform center.

The polar coordinate system determines each point by its radial and angular coordinates denoting the distance from the pole (origin of symmetry) and the angle defined with the polar axis.[23] Let $P(x, y)$ be representation of a point in Cartesian system. Considering (x_o, y_o) as the center of transform, the transform into the polar coordinate is defined by the following equations:

$$r=\sqrt{(x-x_o)^2+(y-y_o)^2},\ 0\le r<\infty \tag{8}$$

$$\theta=\arctan\left(\frac{y-y_o}{x-x_o}\right),\ 0\le\theta\le 2\pi \tag{9}$$

Figure 9b shows the result of transferring Figure 2a into the polar domain using upper left origin detected by our algorithm [marked in Figure 9a] as a transform center. As one can see, streaking artifacts around metal object are converted into the vertical lines in the polar domain. In this way, we can easily remove these artifacts using proper structural element in orthogonal direction[17] without affecting other parts of image.

Morphological filtering

In polar coordinate section, we showed that mapping CBCT image into the polar domain maps streaking artifacts into the vertical lines. These lines can be easily removed

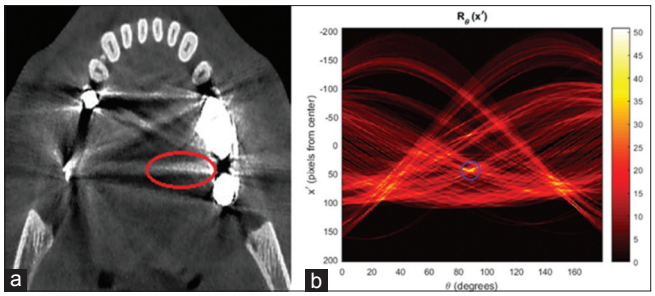

Figure 7: (a) Input image, (b) radon transform of edge map

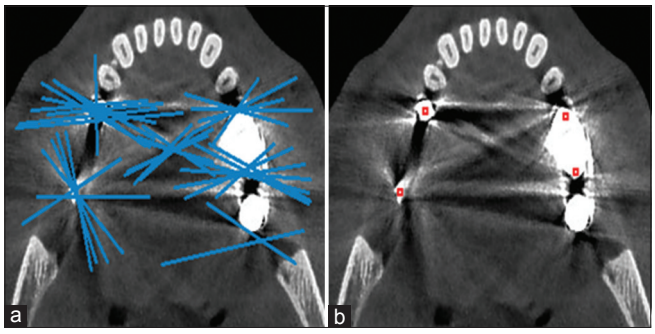

Figure 8: (a) Detected lines, (b) detected streaking artifact origins

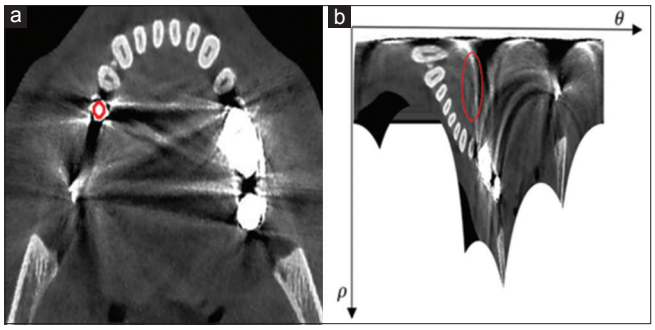

Figure 9: (a) Cartesian coordinate, (b) result of transferring into the polar domain

using morphological filtering. We have used morphological filtering due to its good trade-off between computational complexity and accuracy for removing undesired objects. Mathematical morphology is a tool for extracting image components and morphological filtering for pre- or postprocessing such as eliminating irrelevant objects or emphasizing useful objects.[12] Two basic operators of morphological filtering are erosion and dilation. The erosion $I \ominus S$ of a set I by the structuring element S is defined as the set of shifts z of S for which the shifted set $(S)_z$ is entirely contained in I:[24]

$$I \ominus S := \{z | (S)_z \subseteq I\} \tag{10}$$

The dilation $I \oplus S$ of a set I by S is defined as the set of shifts z of S for which the intersection of I and the shifted S is nonempty:[24]

$$I \oplus S := \{z | (\hat{S})_z \cap I \neq \varnothing\} \tag{11}$$

Combining the dilation and erosion, it is possible to define two new operations. The composition of an erosion with a subsequent dilation is called opening:

$$I \circ S := (I \ominus S) \oplus S \tag{12}$$

The reverse order of the operations is called closing:

$$I \circ S := (I \oplus S) \ominus S \tag{13}$$

Opening removes fine appendages which are thinner than S and preserves (i.e., opens) inclusions, whereas closing preserves fine appendages and closes inclusions thinner than S.[24] Results of morphological filtering depend on the type of filter together with the shape and size of structuring element. Considering streaking artifacts changed into the vertical lines in the polar domain, we can eliminate these artifacts by morphological opening using horizontal line as structural element. Figure 10b shows the result of applying opening morphological filtering on polar domain where vertical lines are removed. Figure 10c shows the reconstructed image after applying inverse Cartesian transform.

After transferring artifact-reduced image into the Cartesian domain (using inverse Cartesian transform), streaking artifacts are removed in the Cartesian domain as shown in Figure 10c. In Figure 10, we have just implemented our method on one of the streaking artifact centers (upper left streaking) and the main part of streaking artifacts around this origin is reduced. Applying similar method for the remaining artifact origins will remove all the streaking artifacts of the image. Result of applying artifact reduction algorithm on all of the artifact origins is demonstrated in Figure 11b. Therefore, the number of required iterations for proposed method to reduce all streaking artifacts is equal to the number of detected streaking artifacts origin as described in automated streaking artifact origin detection section. Note that, morphological opening degrades the quality of teeth in each iteration. This problem is resolved in fusion step.

Cavity filling

In dental CBCT images, cavities are dark regions that appear around teeth and pulp areas. These are also called "missing value artifacts" which appear when the object under study contains highly absorbing material.[10] In this case, the signal recorded in the detector pixels behind that material may be close to zero or actually zero. Naranjo *et al*.[17] proposed to use a simple thresholding method to detect cavities in CT images. Cavities are preserved from the effect of filtering. However, they did not propose a method to remove these cavities on the final reconstructed image. Shape of cavities in CBCT images is more complex than that of the CT images, and simple thresholding (which is applied on the whole image) has a poor performance. Instead, cavities can be detected and removed using local thresholding rather than the global thresholding

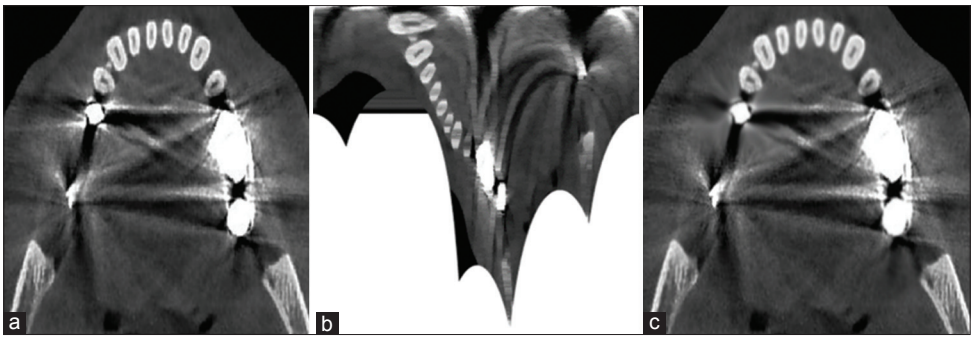

Figure 10: Result of applying morphological opening on streaking artifact reduction (a) Original image, (b) artifact-reduced image in polar domain, (c) artifact-reduced image in Cartesian domain

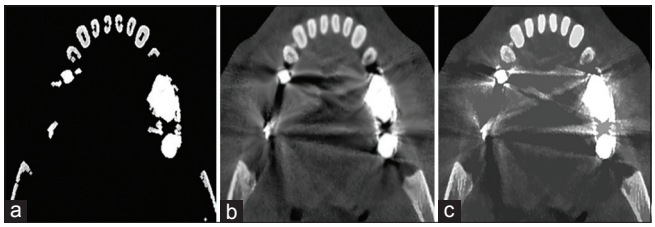

Figure 11: Extracted information from dental cone beam computed tomography image using (a) teeth extraction, (b) streaking artifact reduction, (c) cavity filling

method. Considering hole regions in CBCT images, they are homogeneous regions which have significant intensity drift from neighbor pixels.[25] Based on this nature, we proposed to use morphological region filling[11] to fill cavity areas. Suppose that I is a connected region and let $\mho$ denote the region enclosed by and assume that $I \cap \mho = \emptyset$, beginning with a start point $P \in \mho$, the following iterative algorithm fills all other belonging points to $\mho$. For this purpose, the set F is calculated iteratively using Eq. 14.

$$F_k := \left(F_{k-1} \oplus S\right) \cap \overline{I}, k = 1,2,3,\ldots \quad (14)$$

For the first iteration, F_0 is set to be $\{P\}$. The dilation using S as structuring element results in growth of region and intersection removes possibly added points that do not belong to $\mho$ set. The iteration will terminate as soon as $F_k = F_{k-1}$. This condition shows that all cavity points are included in F set. In order to evaluate the efficiency of morphological filling, the result of filling Figure 2 using Eq. 14 with a disk-shaped structural element is shown in Figure 12. As one can see, all cavities are filled using morphological region filling. Since cavities are different types of artifacts, we have used a different and independent algorithm to remove them. Note that, even though streaking artifacts appeared in Figure 12, they are removed with a different and independent algorithm. In fact, cavity filling and streaking artifact reduction are two independent modules of which one of them removes the effect of cavities (as missing value artifacts) and the other one reduces the effect of streaking artifacts. Each module has its own output and the final fusion step merges these outputs in a way to reconstruct an artifact-reduced image.

Fusion

In previous parts, we explained how to extract teeth, reduce streaking artifacts, and fill cavities of dental CBCT images. However, the information provided in each step is complementary and we need to fuse this information to reconstruct a pleasant image.[26]

Figure 11 shows information extracted from image of Figure 2a in three proposed steps. As demonstrated, extracted information is complement of each other. Therefore, correct fusion of these images can produce an image with good subjective quality. Since teeth are degraded in both streaking artifact reduction and cavity filling steps, in the final image, we have used the information of teeth extraction step to reconstruct this area. Specifically, we have used mask M_t provided in teeth extraction step. In the remaining parts of the teeth, we have used cavity-filled image information for cavity areas and streaking artifact-reduced image for the rest of the image. In order to find the cavity areas, we have simply calculated the difference between original image and cavity-filled image and produce a mask called M_c which is 1 in regions with big difference and 0 on the remaining parts. Since we are using the information of artifact-reduced part for the rest of the image, we have calculated a mask M_{ar} for this area using M_t and M_c as follows:

$$M_{ar} := I - \left(M_t \bigcup M_c\right) \quad (15)$$

Figure 13 shows extracted masks for Figure 2a considering the output of teeth extraction, streaking artifact reduction, and cavity filling steps. Figure 13a shows the mask for teeth extraction which was calculated based on the output of the teeth extraction step. Figure 13b shows the mask for cavity filling which is calculated using the difference between cavity-filled image and the original one. Finally, Figure 13c shows the mask for the streaking artifact reduction step. As mentioned, this mask is calculated based on the teeth extraction and cavity filling masks using Eq. 15.

Fused image is calculated based on the extracted masks:

$$I_f = M_t \circ I + M_c \circ I_c + M_{ar} \circ I_{ar} \quad (16)$$

where I_f is the fused image and I, I_c, and I_{ar} stand for input image, cavity-filled image, and artifact-reduced image,

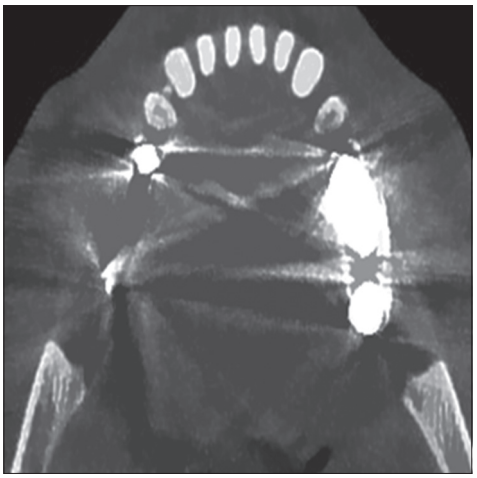

Figure 12: Cavity filling using morphological region filling

respectively. Note that ·o is an element-wise multiplication operator. After calculating fused image, a Gaussian filter is applied on the boundaries of the masks in order to smoothen sudden changes on the boundaries and give a suitable reconstructed image for human visual system.

Figure 14 shows the result of fusion step. Figure 14a shows the extracted component using the teeth extraction step ($M_t \circ I$ in Eq. 16). Figure 14b shows the extracted component from the cavity filling step ($M_c \circ I_c$ in Eq. 16) and Figure 14c is the extracted component from the streaking artifact reduction part ($M_{ar} \circ I_{ar}$ in Eq. 16). Result of the addition of these three components is shown in Figure 14d. Finally, Figure 14e shows the result of applying Gaussian filter on the boundaries of the masks.

Results

Artifact reduction algorithm is implemented on MATLAB (matrix laboratory) is a multi-paradigm numerical computing environment which is developed by MathWorks. Results are provided by a machine with Intel® Xeon® CPU and 64 GB RAM which has a 64 bit operating system. Our proposed method is an application of digital image processing techniques on medical images. Digital images are subject to a wide variety of distortions during acquisition, processing, compression, storage, transmission, and reproduction, any of which may result in a degradation of visual quality.[27] Two types of image quality assessments are subjective and objective evaluation. For applications in which images are ultimately to be viewed by human beings (including our application), the only "correct" method of quantifying visual image quality is through subjective evaluation.[27] Objective quality metrics are developed due to time-consuming and expensive nature of subjective evaluation.[28] The most popular objective image quality metrics are derived based on the available original (distortion free) image. Mean squared error, peak signal-to-noise-ratio, and structural similarity are some of the most well-known metrics in this category.

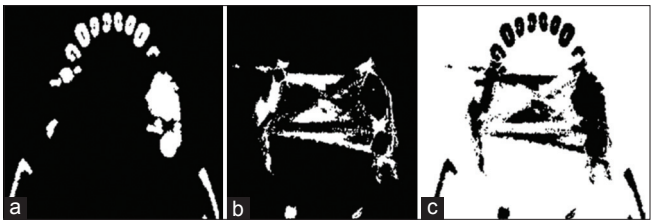

Figure 13: Extracted masks using (a) teeth extraction, (b) cavity filling, (c) streaking artifact reduction

However, due to the nature of our data set, we have no access to distortion-free images. Therefore, this is impossible to use these objective metrics for quality evaluation of reconstructed images and we will use only subjective video quality to evaluate the reconstructed images. In this section, the results of proposed artifact reduction method are provided. First, we will discuss about our data set. In the second part, visual results of applying proposed algorithm on dental CBCT images are provided. Finally, we have evaluated the results of applying proposed method based on the comments of dental expertise.

Data set

We have used a set of 67 patients to provide dental CBCT images. In order to obtain the same thickness, we have used 1-mm cuts in axial region. The specifications of data acquisition tool are demonstrated in Table 1.

Image reconstruction is provided by NNT viewer 2.17 software (Verona, Italy). Reconstructed CBCT images are in JPEG format with three channels representing red, green, and blue components. However, the provided information of all the three channels is same. Therefore, before processing, we have calculated luminance of image and only this component is used to implement proposed artifact reduction algorithm. Figure 15 shows some examples of our data set. As one can see, produced images suffer from severe streaking artifacts and cavities in regions with filling or implants. The strength of artifacts varies based on the scanned area, amount of metal matter existing in the area, and angle of the scanner. Based on the data set, it is worth noting that designing a single algorithm to handle various strengths of artifacts and retain an acceptable quality in reconstructed images is a challenging task.

Visual quality of reconstructed images

Results of applying proposed artifact reduction method are provided here. Considering the disk shape of teeth, we have used a disk-shaped structural element with a minimum size of 2 and maximum size of 5 for morphological filtering as described in teeth extraction section. As mentioned before, after applying polar transform using streaking artifact origin as transform center, streaking artifacts will convert into the vertical lines. Therefore, morphological filtering with line shape structural element and horizontal direction is used in artifact reduction part.

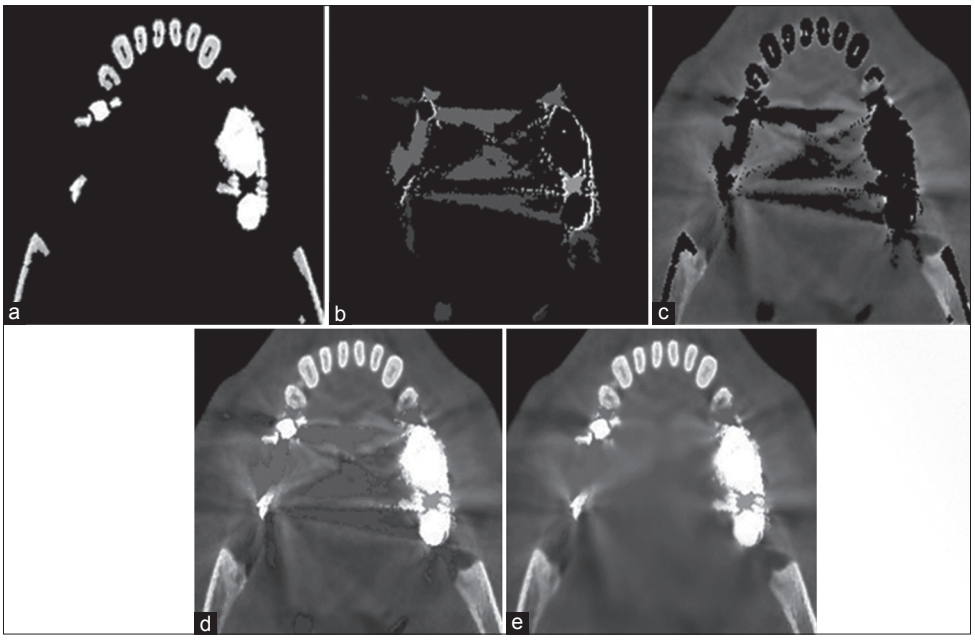

Figure 14: Result of image fusion step (a) extracted teeth, (b) filled cavities, (c) streaking artifact reduction, (d) addition of three extracted components, (e) final reconstructed image using Gaussian filtering on the boundaries of the masks

Table 1: Specifications

Imaging Parameter	Value
Panel resolution	1920×1536
Rotation	360°
Scan	18 s
Maximum voltage	110 KV
Maximum resolution of CBCT images	380×380

CBCT – Cone beam computed tomography

Figure 16 shows some pair of input CBCT images together with related artifact-reduced versions. In each pair, the image in the left side is the original one and the image in the right side is the artifact-reduced one. Considering the results of Figure 16, the proposed algorithm clearly reduces the effect of artifacts on dental CBCT images. Streaking artifacts are significantly reduced owing to good performance of streaking origin detection and converting image into the polar domain. On the other hand, cavities are filled using proposed algorithm which results in a good subjective quality of reconstructed image. It is worth noting that both streaking artifact reduction and cavity-filling steps make some distortion on teeth area. However, we have limited this distortion by accurate extraction of teeth using our histogram-based thresholding. Finally, fusion step has provided a smooth output image with good subjective quality.

As mentioned in data set section, strength of metal artifacts is different for each image. Artifacts of input image in Figure 16d, g, h, and l have low strength. Results show that related reconstructed images have a good visual quality. In these images, artifacts are reduced significantly without any effect on the remaining part of the image. Figure 16a, c, f, i, j, and k shows artifacts with moderate strength. In the related reconstructed image of these images, streaking artifacts are removed and cavities are filled. However, due to stronger artifacts, a bit noisy parts appear in the regions around teeth. These noisy parts are blurred and make no significant degradation on the quality of final reconstructed image. Finally, artifacts in Figure 16b and e are very strong. Even though the proposed algorithm reduced the amount of artifact in these images too, due to strength of these artifacts, some considerable blurring regions are produced.

Check list results

In the previous section, visual quality of the reconstructed images is demonstrated. Since dental CBCT images are ultimately to be used by dental expertise, the proposed method is evaluated based on the comments of dental expertise using a check list of scores for each image. Each check list contains five level of scores in which score 1 is related to the lowest quality of image and score 5 is related to the highest quality of image. Dental expertise scored a set of 65 images. Table 2 shows the percentage of each level in the check list before and after applying proposed algorithm.

As one can see, percentages of images with higher quality (scores 4 and 5) are increased significantly after applying proposed algorithm. We have evaluated the average score of each image before and after applying proposed method. Table 3 shows difference of scores for our data set.

Considering the results of Table 3, expertise evaluated that 4.6% of images have an increase of 2 in quality

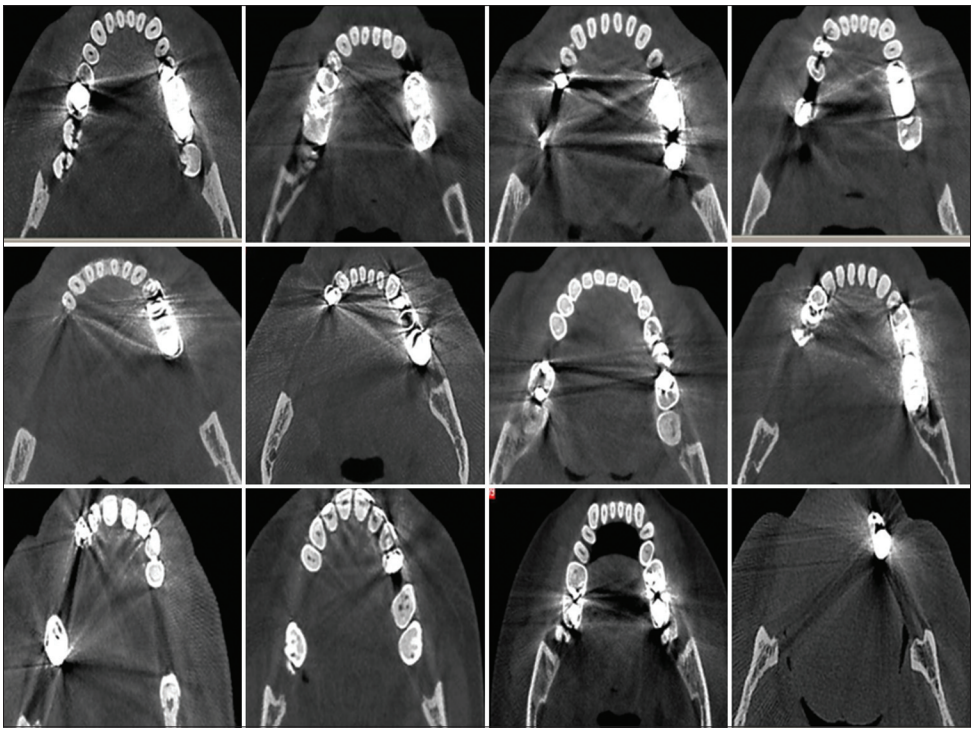

Figure 15: Dental cone beam computed tomography images for artifact reduction

score, 66.2% of images have an increase of 1 in quality score, 27.7% of images have no change in image quality, and 1.5% of images decrease in quality by a score of 1. On an average, the quality of images has a score of 2.91 ± 72 before applying proposed algorithm and quality of 3.64 ± 0.62 which shows an increase of 0.73 in quality score. Average values of scores together with the corresponding SD are shown in Figure 17.

Due to nonnormal distribution of scores, we have used Wilcoxon signed-rank test[29] to compare images before and after applying proposed algorithm. Table 4 shows results of our statistical analysis.

Considering $P < 0.001$, Wilcoxon signed-rank test shows that there is a meaningful difference between CBCT dental images before and after applying proposed algorithm.

Comparison with conventional methods

In this section, proposed method is compared with two well-known image denoising techniques, namely discrete wavelet transform (DWT)-based artifact reduction method[30,31] and discrete cosine transform (DCT)-based artifact reduction method.[32,33] In the first method, different families of wavelets including Haar, Daubechies, Coiflets, and Symlets are used to process the set of dental CBCT image. Daubechies filter (db2) obtained the best results and was used in comparison. Two types of coefficient thresholding, namely hard and soft threshold, are performed on denoising. In both schemes, threshold is calculated based on the image variance. The best results were obtained for the soft threshold. Regarding DCT-based method, parameters are tuned to obtain best results. Specifically, the size of the DCT block is set to $N = 8$ and soft threshold is chosen for the coefficient thresholding. Figure 18 shows a comparison between reconstructed images of our method and the image denoising algorithms described above, using the parameters for which the best results have been

Table 2: Scores before and after applying proposed algorithm

Score	Before	After
1	0	0
2	30.8	3.1
3	47.7	33.8
4	21.5	58.5
5	0	4.6

Table 3: Difference of scores for our data set

Score difference	Percentage
−1	1.5
0	27.7
1	66.2
2	4.6

Table 4: Statistical analysis results

	Mean±SD	Mean difference	Wilcoxon signed-rank test	*P*
Before	0.72±2.91	0.73±0.57	−6.4	<0.001
After	0.62±3.64			

SD – Standard deviation

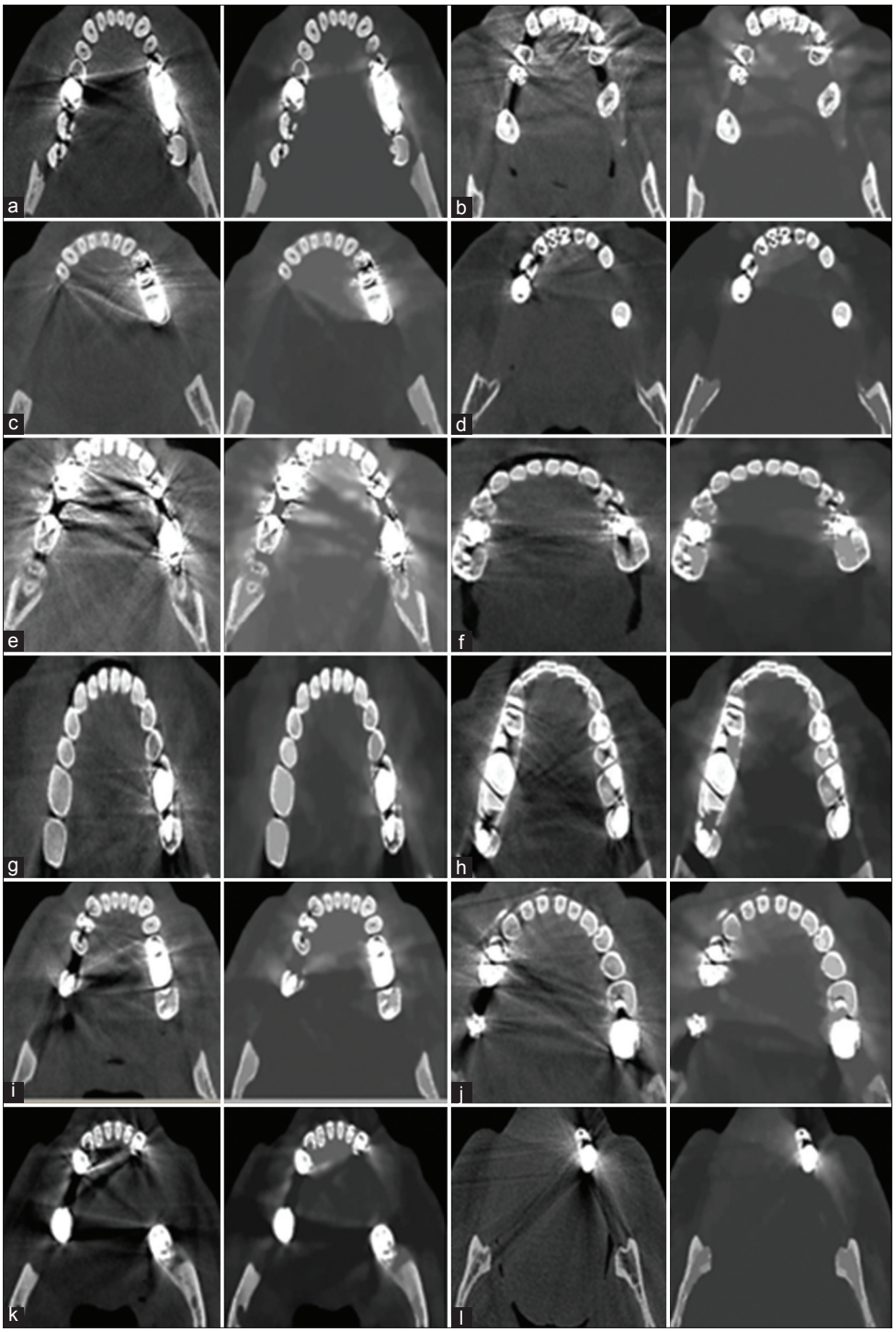

Figure 16: (a-l) from left to right: Dental CBCT image and its artifact reduced version using proposed algorithm. Result of applying artifact reduction method on cone beam computed tomography images

achieved. In each row of Figure 18, the first image from the left is original image. The second, third, and fourth images are reconstructed images using proposed method, DWT-based and DCT-based image denoising methods, respectively. As one can see, DWT- and DCT-based images can remove some high-frequency components of artifacts; however, the main part of the artifacts remains. Proposed method gives superior subjective quality compared to DWT- and DCT-based methods. In Figure 18b, artifacts are not strong enough and reconstructed images by DWT- and DCT-based methods have an acceptable quality. However, in Figure 18a and c, where artifacts are moderate and high, respectively, DWT- and DCT-based methods failed to remove the artifacts. Superior performance of the proposed method is because of intelligent use of histogram information and symmetric nature of streaking artifacts.

Conclusion

In this article, we have proposed an algorithm to reduce artifact of dental CBCT images. In contrast to previous CBCT artifact reduction algorithms which make modifications on data acquisition part, our algorithm is completely dependent of data acquisition and is based on image processing techniques. Dental CBCT images suffer from severe streaking artifacts and cavities around teeth.

In order to decrease these artifacts and create a visually good image, we have proposed three independent and parallel components: teeth extraction component extracts teeth using an adaptive threshold which is based on the histogram, image histogram is modeled using a one-dimensional GMM and threshold is defined based on GMM parameters, and streaking artifact reduction component uses symmetry of artifacts around artifact origin. The first artifact origins are calculated using Radon transform-based line detection and finding intersection of the lines. After finding streaking artifact origins, image is transformed into the polar domain using each origin as a transform center. This converts all streaking artifacts around that point into the vertical lines which can be easily removed using morphological opening. Cavity filling component uses simple morphological filling to fill cavities. After applying each component, we have three images with different information. Fusion step combines these images and produces a single image which contains information of all components. Results show that proposed algorithm has a promising performance for artifact reduction of dental CBCT images. Streaking artifacts are reduced significantly in output image and cavities around teeth are filled with proper intensity value.

Proposed algorithm is completely independent from data acquisition step. Therefore, it can be applied on dental CBCT images acquired from any tool. On the other hand, it can be used along with the artifact reduction algorithms which make modification on data acquisition part. In this way, we can achieve even better results.

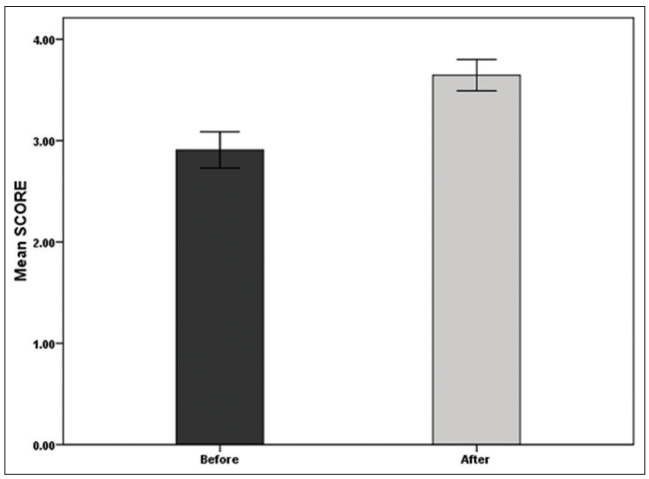

Figure 17: Average quality score of dental cone beam computed tomography images before and after applying proposed algorithm

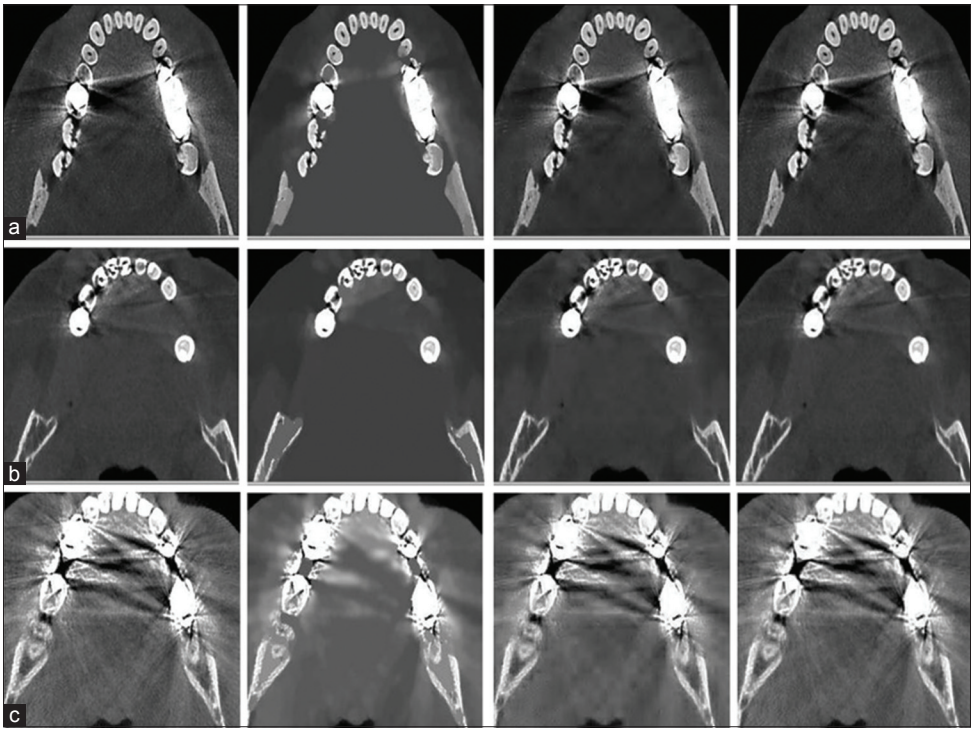

Figure 18: (a-c) Dental CBCT image and the result of applying artifact reduction using proposed algorithm, DWT-based noise reduction and DCT-based artifact reduction, respectively (from left to right). Comparison of proposed method with discrete wavelet transform and discrete cosine transform-based image denoising methods

Financial support and sponsorship

None.

Conflicts of interest

There are no conflicts of interest.

References

1. Hassan B, Jacobs R. Cone beam computed tomography-3D imaging in oral and maxillofacial surgery. Eur Med Imaging Rev 2008;1:38-40.
2. De Man B, Nuyts J, Dupont P, Marchal G, Suetens P. Metal streak artifacts in X-ray computed tomography: A simulation study. IEEE Trans Nucl Sci 1999;46:691-6.
3. Nakae Y, Sakamoto K, Minamoto T, Kamakura T, Ogata Y, Matsumoto M, *et al.* Clinical evaluation of a newly developed method for avoiding artifacts caused by dental fillings on X-ray CT. Radiol Phys Technol 2008;1:115-22.
4. Barrett JF, Keat N. Artifacts in CT: Recognition and avoidance. Radiographics 2004;24:1679-91.
5. Wang Q, Li L, Zhang L, Chen Z, Xing Y, Kang K. Reducing Metal Artifacts by Pre-processing Projection Data in Dental CBCT with a Half-size Detector. In: Nuclear Science Symposium and Medical Imaging Conference (NSS/MIC), 2011 IEEE; 2011. p. 3434-7.
6. Goldman LW. Principles of CT: Radiation dose and image quality. J Nucl Med Technol 2007;35:213-25.
7. Pauwels R, Stamatakis H, Bosmans H, Bogaerts R, Jacobs R, Horner K, *et al.* Quantification of metal artifacts on cone beam computed tomography images. Clin Oral Implants Res 2013;24 Suppl A100:94-9.
8. Imai K, Ikeda M, Enchi Y, Niimi T. Statistical characteristics of streak artifacts on CT images: Relationship between streak artifacts and mA s values. Med Phys 2009;36:492-9.
9. Sanders MA, Hoyjberg C, Chu CB, Leggitt VL, Kim JS. Common orthodontic appliances cause artifacts that degrade the diagnostic quality of CBCT images. J Calif Dent Assoc 2007;35:850-7.
10. Schulze R, Heil U, Gross D, Bruellmann DD, Dranischnikow E, Schwanecke U, *et al.* Artefacts in CBCT: A review. Dentomaxillofac Radiol 2011;40:265-73.
11. Soille P. Morphological Image Analysis: Principles and Applications. Springer-Verlag Berlin Heidelberg: Springer Science & Business Media; 2013.
12. Gonzalez R, Wintz P. Digital Image Processing. Pearson, US; 1977.
13. Zivkovic Z. Improved adaptive Gaussian mixture model for background subtraction. In: Pattern Recognition, 2004. ICPR 2004, Proceedings of the 17th International Conference on, IEEE. Vol. 2. 2004. p. 28-31.
14. Lee DS. Effective Gaussian mixture learning for video background subtraction. IEEE Trans Pattern Anal Mach Intell 2005;27:827-32.
15. Moon TK. The expectation-maximization algorithm. IEEE Signal Process Mag 1996;13:47-60.
16. Otsu N. A threshold selection method from gray-level histograms. IEEE Trans Syst Man Cybern 1979;9:62-6.
17. Naranjo V, Lloréns R, Alcañiz M, López-Mir F. Metal artifact reduction in dental CT images using polar mathematical morphology. Comput Methods Programs Biomed 2011;102:64-74.
18. Haralick RM, Sternberg SR, Zhuang X. Image analysis using mathematical morphology. IEEE Trans Pattern Anal Mach Intell 1987;9:532-50.
19. Gonzalez CI, Melin P, Castro JR, Mendoza O, Castillo O. An improved Sobel edge detection method based on generalized type-2 fuzzy logic. Soft Comput 2016;20:773-84.
20. Deans SR. The Radon Transform and Some of Its Applications. Mineola, Dover Publications, INC: Mineola, New York; Courier Corporation; 2007.
21. Murphy LM. Linear feature detection and enhancement in noisy images via the Radon transform. Pattern Recognit Lett 1986;4:279-84.
22. Zhang Q, Couloigner I. Accurate centerline detection and line with estimation of thick lines using the radon transform. IEEE Trans Image Process 2007;16:310-6.
23. Hanbury A, Serra J. Colour image analysis in 3D-polar coordinates. In: Joint Pattern Recognition Symposium. Springer-Verlag Berlin Heidelberg; 2003. p. 124-31.
24. Beyerer J, León FP, Frese C. Machine Vision: Automated Visual Inspection: Theory, Practice and Applications. Springer-Verlag Berlin Heidelberg; 2015.
25. Liu R, Miao Q, Huang B, Song J, Debayle J. Improved road centerlines extraction in high-resolution remote sensing images using shear transform, directional morphological filtering and enhanced broken lines connection. J Vis Commun Image Represent 2016;40:300-11.
26. Abdollahzadeh M, Malekzadeh T, Seyedarabi H. Multi-focus Image Fusion for Visual Sensor Networks. In: Electrical Engineering (ICEE), 2016 24th Iranian Conference on, IEEE; 2016. p. 1673-7.
27. Wang Z, Bovik AC, Sheikh HR, Simoncelli EP. Image quality assessment: From error visibility to structural similarity. IEEE Trans Image Process 2004;13:600-12.
28. Wang Z, Bovik AC, Lu L. Why is image quality assessment so difficult? In: Acoustics, Speech, and Signal Processing (ICASSP), 2002 IEEE International Conference on, IEEE. Vol. 4. 2002. p. IV-3313-6.
29. Woolson R. Wilcoxon signed rank test. Wiley Encyclopedia of Clinical Trials. John Wiley & Sonc, Inc; 2008.
30. Yoon BJ, Vaidyanathan PP. Wavelet-based denoising by customized thresholding. In: Acoustics, Speech, and Signal Processing, 2004. Proceedings.(ICASSP'04). IEEE International Conference on, IEEE. Vol. 2. 2004. p. ii-925.
31. Zhao S, Robertson DD, Wang G, Whiting B, Bae KT. X-ray CT metal artifact reduction using wavelets: An application for imaging total hip prostheses. IEEE Trans Med Imaging 2000;19:1238-47.
32. Yaroslavsky L, Egiazarian K, Astola J. Transform domain approaches for image denoising. J Electron Imaging 2002;11:149-56.
33. Tuna U, Ruotsalainen U. Metal Artifact Reduction with DCT-domain Gap-filling Method. In: Nuclear Science Symposium and Medical Imaging Conference (NSS/MIC), 2012 IEEE. IEEE; 2012. p. 2322-4.